Jurnal Kejuruteraan 36(5) 2024: 1973–1987
https://doi.org/10.17576/jkukm-2024-36(5)-17

Synchronization of Phase and Frequency in Flyback Inverter Using a New Ripple Hysteresis Controller

Gongzhuo Chen, Radin Za`im & Yushaizad Yusof*

Department of Electrical, Electronics & System Engineering,
Faculty of Engineering & Built Environment,
Universiti Kebangsaan Malaysia, Malaysia

**Corresponding author: yushaizad@ukm.edu.my*

Received 8 November 2023, Received in revised form 26 May 2024
Accepted 26 June 2024, Available online 30 September 2024

ABSTRACT

In this paper, a novel approach called ripple hysteresis controller (RHC) is proposed. Previously current signal and hysteresis band are controlled independently in the hysteresis conventional controller (HCC). However, the HCC are unable to achieve a stable current frequency due to the current signal inside the hysteresis band is less immune to disturbance and fluctuates when external signals interfere with it. To solve the problem of HCC inability to effectively control the frequency and phase of the current signal, the RHC is introduced. It is based on a novel double closed-loop control model. Firstly, a closed-loop control is carried out to compare and evaluate the frequency variation and phase synchronization of the magnetizing current. Secondly, the closed-loop control is utilised to control the hysteresis controller band. The new RHC approach is demonstrated using the MATLAB Simulink tool to substantially reduce the output ripple error of current and voltage as well as to enhance the transition accuracy at zero crossing in comparison to the HCC. This study focuses on the mathematical foundations of RHC, simulation design and result analysis. The results of the simulation illustrate the effectiveness of this innovative RHC in overcoming varying frequency and phase. In conclusion, this novel method has successfully validated the proposed RHC performance for flyback inverter application and demonstrated its superiority over HCC in several aspects.

Keywords: Hysteresis controller; ripple; flyback circuit; phase synchronization; magnetizing current

INTRODUCTION

In the case of circuit systems, electricity is an essential source of energy, and electric current is the carrier that delivers the energy. Therefore, controlling the current to provide a pure and stable current is crucial. Frequency and phase are important parameters to evaluate the current performance. In power converter application, one of its vital components is the switching scheme. With proper and correct switching scheme, the switching devices can operate according to the predetermined control method. In power converters operation, there are several switching schemes available, mainly dominated by the pulse width modulation (PWM) techniques (Yusof & Nasrudin 2011; Zainuri et al. 2019). Recently, the hysteresis control is widely used in circuit systems due to its simplicity and rapid response (Komurcugil et al. 2017; Wang et al. 2019;). Continuous Conduction Model (CCM) is used to operate the Hysteresis Conventional Control (HCC) (Lee et al. 2016; Za'im et al. 2019), and the use of hysteresis bands is the core concept of hysteresis control. The hysteresis band defines the range or margin around the desired setpoint value. The control system continuously monitors the process variable (controlled quantity such as temperature, speed or voltage). When the process variable exceeds the upper limit of the hysteresis band, a control action is triggered to switch on the control element.

Hysteresis control has received much attention from the researchers due to its simplicity making its concepts is easily understood. Through examining contemporary

hysteresiscontroller research, three major groups of studies on improving the effectiveness of hysteresis controller are briefly presented as follows:

1. Improved hysteresis controller design for various circuit system configurations. In this aspect, hysteresis control is utilised to enhance the performance of specific kind of system application (Wang et al. 2019; Li et al. 2023; Dong et al. 2023). For instance, a hysteresis control technique for multilayer converters is suggested by dynamically altering the inductor current rotation rate. A hybrid modulation-based hysteresis control technique is proposed to address the efficiency of the grid power conversion issue. A multi-power stage hysteresis control technique for DC-DC converters is reported (Ghani et al. 2022). Additionally, a DC-DC dual inverter control approach using zero sequence current hysteresis control has been developed (Can, 2019). To improve the energy efficiency of the system's storage, a straightforward multimode hybrid hysteresis control mechanism is also suggested.
2. Improved hysteresis current controller using variety of different intelligent algorithms. A wide range of hysteresis control algorithms is to be next in line for current research. Some examples of algorithms include the particle swarm optimisation technique, the predictive hysteresis control method, the dual-band hysteresis current control algorithm, the variable hysteresis band control algorithm, and the hysteresis fuzzy controller (Peter et al. 2020; Feng et al. 2021; Yan et al. 2023).
3. Optimization and adjustment of the parameters of the hysteresis controller independently is proposed to achieve improved control performance. Several methods have been proposed for enhancing the hysteresis controller for the parameters that it possesses independently with the external factors (Kapat et al. 2017; Repecho et al. 2017; Liang et al. 2023). For instance, hysteresis control can be implemented without the hysteresis bands. The control of hysteresis current involves regulating a switching frequency that remains close to a constant value. Moreover, various techniques exist for simulating the change in the hysteresis band through segmentation. An alternative approach to hysteresis control involves augmenting the number of hysteresis bands to enhance current stabilization.

These developments of hysteresis controllers demonstrate the present advancements in control efficacies and hysteresis control technologies. Through comparative analysis, it can be understood that the current hysteresis controller technology can rely on computer algorithms to assist in frequency and phase control management. The inability of conventional hysteresis band to regulate the current frequency has been addressed and discussed in this paper. Nevertheless, the benefit of the hysteresis controller's straightforward construction is eliminated by the complex circuit design. Moreover, the control effect of the voltage zero-crossing point is not fully considered by the recent hysteresis controllers. In applications, the majority of the recently developed hysteresis controllers have satisfied the demands of large-scale machinery for high precision and online networking adaptability. However, complex circuits are not suitable for the development of small devices such as microinverters. In general, although the research on hysteresis controllers in recent years has improved the performance of the controllers, there still has some space for improvement in terms of configuration, efficiency and in high switching frequency application. Therefore, a novel idea is required to fulfil the high precision requirements for current frequency and phase, as well as to address the research gap of hysteresis controllers in small devices. In addition, it preserves several benefits of the conventional hysteresis controller's straightforward construction.

Although various improvement of hysteresis controls mentioned earlier help to improve the control performance of a circuit system, hysteresis control still has an obvious disadvantage that needs to be addressed. In other words, since hysteresis controller cannot regulate the frequency of the current signal, it cannot control the phase of the current signal, and the current signal flows through the hysteresis region ends up with a large error which will cause substantial losses. Besides, PWM controllers which are widely used, has several advantages (Shi et al. 2023). The PWM controller output is a fixed-frequency pulse signal, which results in a fixed current phase and frequency with a very minimum output voltage inaccuracy. However, it is obvious that PWM controllers have several drawbacks also. The PWM controllers contain additional complex circuits with more conditions compared to the hysteresis controllers, which causes the system to respond slower (Yusof & Nasrudin 2011). The idea to combine the constant frequency advantage of PWM controller with simple operation and fast response speed superiority of hysteresis controller can trigger a significant challenge. In addition, a phase synchronization method for intermittent or boundary conduction mode (BCM) that have successfully reduced the generation of switching current ripple has been proposed (Sibanyoni et al. 2019; Zhang et al. 2019). On the other hand, a simple technique was introduced to control the magnetizing current of a flyback inverter circuit (Za'im et al. 2019).

Through analytical arguments, this paper proposes and discusses about a new ripple hysteresis controller (RHC)

for the flyback inverter circuit. It introduces a new design for hysteresis control technique. The design employs a dual closed-loop control circuit where a closed-loop magnetizing current circuit is connected to a closed-loop hysteresis band circuit, while phase filtering of the magnetizing current is applied to refine the current frequency. The closed-loop output signal is subsequently fed into the hysteresis band so that the signal with a specific frequency is triggered when the current signal is applied in the hysteresis band. With the utilization of closed-loop control to the hysteresis band, the system error will be reduced, and will result in considerable improvement for system performance. By controlling the frequency and phase of the magnetizing current, the losses as well as voltage harmonic distortion can be reduced. The effective reduction of the total harmonic distortion (THD) in the sinusoidal output voltage as well as the output current can be achieved through precise control of frequency and phase. The attainment of lower THD values holds significant importance for enhancing the power quality as well as improving the safety of electrical circuit. Therefore, the newly proposed RHC is assumed to be more effective in tackling the issues pertinent to the HCC. The fixed frequency and phase can accurately help in calculating the critical circuit parameters such as magnetizing inductance, capacitance and others, as compared to those using the HCC. Thus, it helps the researchers to improve their circuits' performance and can contribute significantly to the advancement of hysteresis control.

The flyback inverter circuits work very efficiently in the power grid (Za'im et al. 2022). According to Bhattacharya et al. 2023, the flyback inverter circuit magnetizing current phase control is a crucial part. Since the flyback inverter circuits are rarely utilized alone and most of them are multiple-stage parallel flyback circuits, which will make the branch circuit current phase control rather troublesome. Therefore, the flyback inverter circuit has been chosen as a perfect testing environment for the proposed novel ripple hysteresis model theory. The flyback inverter circuit as depicted in Figure1 serves as the basis for this work. It utilizes two GaNs and four MOSFETs switching devices with two switching transformers.

The goal of this paper is to design, simulate and analyze the proposed ripple hysteresis controller for flyback inverter circuit. Furthermore, to validate the improved performance of RHC against the HCC is subject to magnetizing current phase synchronization and constant frequency simulation findings. Thereby, this paper is organized as follows: Section 2 explains the methodology, which provides the system design, principle of operation, design procedure and initial information regarding the proposed controller. Section 3 showcases and demonstrates the simulation results, whereas Section 4 analyzes and discusses the findings as well as compares the performance of the proposed RHC and the HCC. Finally, this paper is concluded in Section 5.

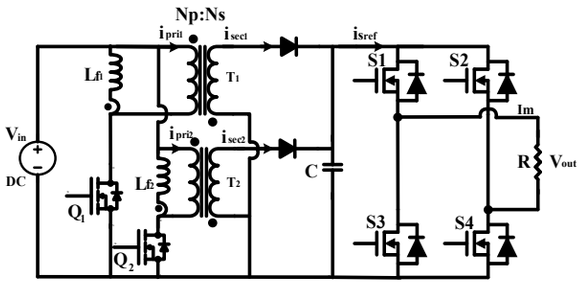

FIGURE 1. Flyback inverter schematic circuit

METHODOLOGY

SYSTEM DESIGN

This study used MATLAB Simulink software tool (Matharani & Jariwala 2024), to model the flyback inverter circuit and to simulate the findings. It has been applied in building, modelling and testing the flyback inverter circuit based on the predetermined system parameters. To conduct faster and accurate simulation work, a discrete model is developed. The new RHC, is required to solve the problem of large errors due to frequency instability. Within the framework of this study, the proposed RHC is characterized by the integration of a sophisticated double-control feedback system. The proposed technique is based on a closed-loop control mechanism for hysteresis band to achieve a higher accuracy. The double closed-loop hysteresis control circuit logic diagram is illustrated in Figure2. It contains the combination of a phase control loop and a hysteresis band control loop respectively.

The phase control loop reference is the system frequency. Firstly, a phase detector is used to measure the magnetization current signal to obtain the phase waveform from the magnetization current signal. Then, the phase waveform is filtered using a low-pass filter and the resulting frequency is digitized as the value of phase after being compared to the system frequency signal. The hysteresis band control's reference is based on a sinusoidal waveform magnetizing current signal. After being compared to the measured actual magnetizing current signal, the resulting error is fed into the hysteresis band. Subsequently, the digitized phase signal waveform is fed into the ripple hysteresis controller to successively update the phase as well as the frequency of the controlled magnetizing current signal.

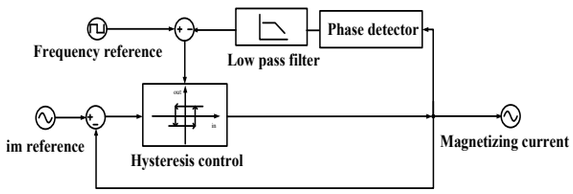

FIGURE 2. A proposed ripple hysteresis control system

PRINCIPLE OPERATION OF PROPOSED CONTROLLER

HYSTERESIS CONVENTIONAL CONTROL

The hysteresis conventional control (HCC) begins with defining a setpoint, which is the desired value for the controlled variable. Next, the intricate arrangement of hysteresis control authorizes the incorporation of two critical limit values: the upper limit, denoted as U and the lower limit, denoted as L respectively. These limits hold primary significance in governing the precise timing of control actions within the system. Specifically, the upper threshold (U) serves as the delineation point at which the system activates a control action to ensure the controlled variable remains within the specified upper limit, thus preventing potential overruns. Conversely, the lower threshold (L) plays an equally pivotal role by which the system activates a control action to sustain the controlled variable within the specified lower limit.

Figure 3 illustrates the operating waveforms of the hysteresis control system during a switching cycle. The t_{on} denotes the period when switching device is turn-on, while t_{off} denotes the period when the switching device is turn-off. Therefore, when the magnetizing current signal touches the upper or lower limit, the switching device immediately turn into off state. The switching device remains turn-on when the magnetizing current signal moves forward within the hysteresis control band.

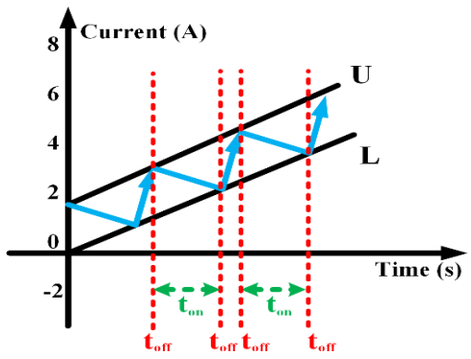

FIGURE 3. Hysteresis control operating condition

PHASE SELECTOR

A S-R latch can be implemented with ease using straightforward logic gates for phase selector. The S-R latch has a capacity to store one bit of data and hold onto that state until the input signal changes value, which precisely parallel with phase selection requirement. It was chosen to decide the difference between the magnetizing current signal and the hysteresis control lower band. Based on the leading-edge rising trigger principle, when the set input is triggered, the phase waveform is also triggered simultaneously. On the other hand, the phase waveform resets to zero when the reset input is activated (Ma et al. 2020). The objectives of the implementation of S-R latch are to guarantee the circuit stability and to maintain simplicity. As a result, it is highly adaptable to various logic circuit systems.

LOW-PASS FILTER

The Sallen-Key low-pass filter (LPF) is selected as a tool for low pass filtering action due to its simplicity, flexibility and accurate control of filter properties. The frequency filtering function is implemented using an operational amplifier and several passive components like resistors and capacitors (Wang et al. 2020). Figure 4 shows the configuration of the Sallen-key low-pass filter. Using the voltage input and output signals, resistors and capacitors, the mathematical formulas for the cut-off frequency, transfer function and quality factor Q can be expressed.

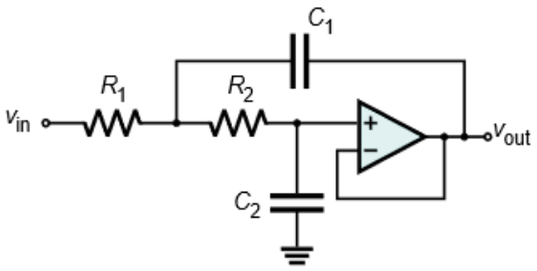

FIGURE 4. Sallen-key low pass filter schematic circuit

The equation for the cut-off frequency, f_c is indicated as follows,

$$f_c = \frac{1}{2\pi\sqrt{R_1 C_1 R_2 C_2}} \quad (1)$$

The second order transfer function of V_{out} and V_{in} as well as the quality factor Q are presented as,

$$\frac{V_{out}}{V_{in}} = \frac{2\pi f_c}{s^2 + 2\zeta(2\pi f_c)s + (2\pi f_c)^2} \quad (2)$$

$$Q = \frac{1}{2\zeta} \quad (3)$$

where ζ is damping ratio.

PHASE SHIFT

The phase shift of 180º is instrumental in balancing the magnetizing current and reducing ripples in the output voltage. This leads to elimination of the voltage and current distortion issues. The off-set time between different magnetizing current frequencies is set to achieve a right phase shift, which can be accomplished using the following equation,

$$T_{off-set} = \frac{1}{2f_{sw}} \quad (4)$$

where f_{sw} is the switching frequency of the circuit system set. Previously mentioned components are utilized to design the RHC based on the parallel flyback circuit. It directly affects the phase and frequency of hysteresis ripple band in controlling the frequency of magnetizing current.

PHASE CONTROL HYSTERESIS BAND

As shown in Figure 5, the magnetizing current variation, Δ_{i_m} is added into the hysteresis band within the closed-loop control system of phase.

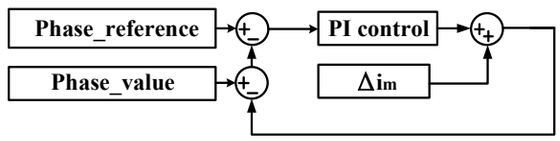

FIGURE 5. Proposed phase control system for hysteresis band

SIMULATED FLYBACK INVERTER CIRCUIT

Figure 6 illustrates a basic configuration circuit for the simulation work. It consists of parallel flyback, H-bridge inverter, resistive load and block diagrams for control system (Chen et al. 2021).

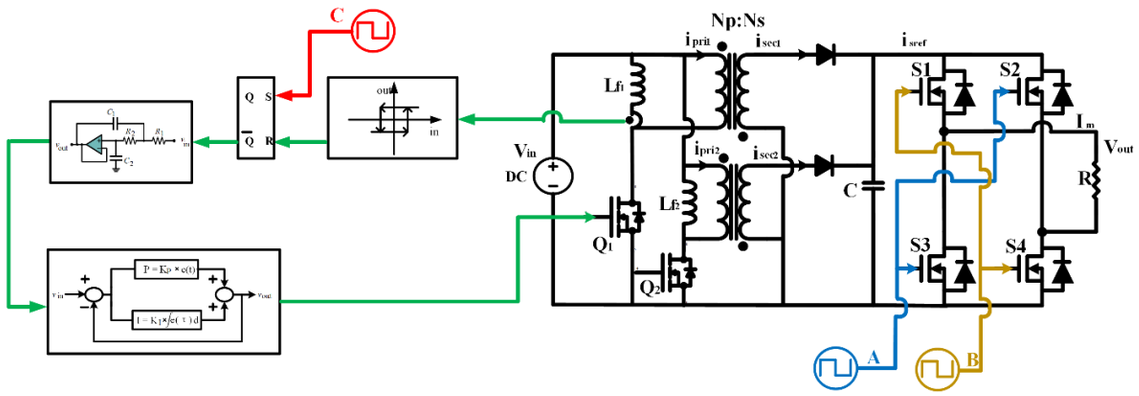

FIGURE 6. Flyback inverter circuit with the proposed ripple hysteresis controller

The RHC control circuit consists of two identical double closed-loop hysteresis control circuits that are coupled to the circuit's switching devices, Q_1 and Q_2 respectively. The i_{m_1} and i_{m_2} are respectively stand for each magnetizing current signal in two loops. The control system of the double closed-loop hysteresis control circuit Q_1 is shown in Figure 6. Therefore, in the simulation work for both Q_1 and Q_2 utilize the exact same control system.

A, *B* and *C* are decent pulse train signal generators, whereby the pulse signal generation is illustrated in Figure 7. Switching frequencies are assigned via repeating sequence with two complement constant inputs, which are set alternately between 0 and 1. Signal generator *C* generates the flyback switching frequency of 200 kHz with 50 percent duty cycle. While the inverter switching frequencies of 50 Hz with a constant 50 percent duty cycle are generated by respective *A* and *B*. Since the respective

switching devices combination of S_1S_4 and S_2S_3 are complementary, thus the *A* and *B* signal generators must have opposite values.

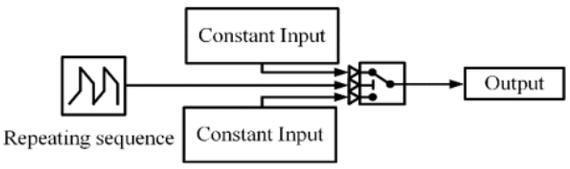

FIGURE 7. Principle of pulse signal generation

The magnetizing current equation is derived in accordance with the circuit configuration and expressed as follows,

$$i_{m_{ref(k)}} = I_m * sin(wt) * \left[\frac{N_S}{N_P} + \frac{|V_g|}{V_d}\right] \quad (5)$$

$$V_{g(k)} = 240\sqrt{2} * \sin(wt) \quad (6)$$

$$I_m = \frac{V_{out}}{R} \quad (7)$$

$$i_{s_{ref(k)}} = I_m * \sin(wt) \quad (8)$$

where N_p is the value of the transformer's primary side, N_S is the value of the secondary side, and $i_{s_{ref}}$ is the secondary circuit's average current. From the preceding study, the i_m moves forward inside the hysteresis control bands as depicted in Figure 8.

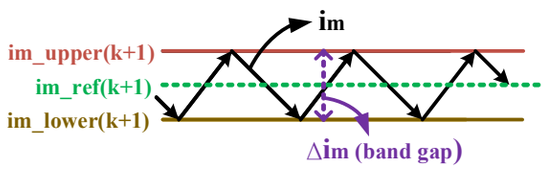

FIGURE 8. i_m signal behaviour inside hysteresis bands

The following formula is used to compute vital parameters and variables such as magnetizing current references, $i_{m_{ref(k)}}$ and the secondary current, $i_{s_{ref(k)}}$ as well as the amplitude, I_m. These will allow for the calculation of updated current value and the subsequent analysis of the current's phase and frequency. The parameters of the circuit system and hysteresis controller used in this work are shown in Table 1 and Table 2 respectively.

$$i_{m_{ref(k+1)}} = \left|\frac{i_{s_{ref(k)}} * N_s}{N_p} \Big/ \left(1 - \frac{V_{g(k+1)} * N_s}{N_s * V_d + V_{g(k+1)} * N_p}\right)\right| \quad (9)$$

$$\Delta_{i_m} = \frac{V_{g(k+1)} * i_{s_{ref(k+1)}}}{f_{sw} * L_m * i_{m_{ref(k+1)}}} + phase \quad (10)$$

$$i_{m_{ref\_upper(k+1)}} = i_{m_{ref(k+1)}} + \frac{\Delta_{i_m}}{2} \quad (11)$$

$$i_{m_{ref\_lower(k+1)}} = i_{m_{ref(k+1)}} - \frac{\Delta_{i_m}}{2} \quad (12)$$

$$L_m = N_p{}^2 * Al \quad (13)$$

where L_m is the magnetizing inductance and Al denotes the inductance factor.

$$V_{g(k)} = |240\sqrt{2} * \sin(wt)| \quad (14)$$

$$i_{s_{ref(k+1)}} = |I_m * \sin(wt)| \quad (15)$$

TABLE 1. Parameters of flyback inverter circuit

Parameter	Symbol	Value
Transformer turn ratio	n	1.67
Magnetizing inductance	L_{f1}	30 µH
Magnetizing inductance	L_{f2}	28 µH
Filter capacitor	C_1, C_2	0.001 µF
Flyback capacitor	C	0.01 µF
Filter resistor	R_1, R_2	2 kΩ
Load resistor	R	100 Ω

TABLE 2. Parameters of hysteresis controller

Parameter	Symbol	Value
Voltage input	V_{in}	24 V
Voltage output	V_{out}	240 V_{rms}
Grid frequency	f_g	50 Hz
Switching frequency	f_{sw}	200 kHz

RESULTS

PHASE SYNCHRONIZATION

Phase selector is used to the detect the phase of magnetizing current, i_m. The sensed i_m is transformed into pulse signal by the phase selector block. The phase is synchronously activated to one when the set signal is triggered (lower

figure) and returns to zero when the reset signal is triggered (upper figure) as depicted in Figure 9. The repetition of the procedure is required to acquire the synchronized phase waveform sequentially. The reset signal is specified as the lower band of the hysteresis control while the set signal is set as the upper band.

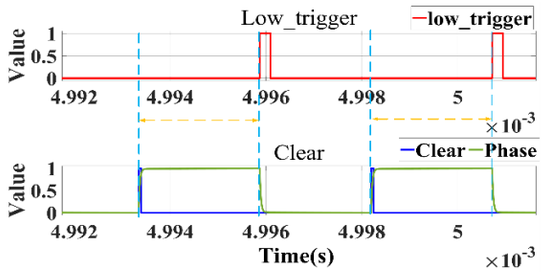

FIGURE 9. Synchronous phase signals

PHASE SIGNAL WAVEFORM FILTERING

Since square waves equations are difficult to derive, hence, they must be filtered into sine wave first using the Sallen-Key LPF. The phase of cut-off frequency for the second order LPF is typically selected at phase angle -90º. Meanwhile, the phase angle shift occurs when the LPF attenuates the signal to 70.7% (or approximately -3 dB) from its maximum value (0 dB). Thus, to determine the resistances and capacitances values, the cut-off frequency, f_c is set at 100 kHz.

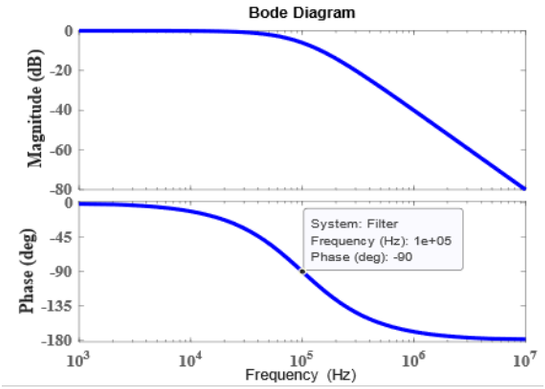

FIGURE 10. Magnitude and phase responses

Figure 10 shows the Bode diagram frequency response of the square wave input signal after being filtered by the LPF. The filtered waveform cut-off frequency of 100 kHz is clearly intersecting the -90º. Since the amplitude range of the input pulse signal is between 0 to 1, whereas the phase at the cut-off frequency is half of the phase period. Hence, the value of phase transformed from analogue signal to the digital signal is 0.5. Figure 11 illustrates the resulting relationship between the respective pulse signal and filtered signal of phase waveform. Apparently, the phase1 signal and phase2 signal are shifted 180º between them. Moreover, the pulse signal phase is shifted 90º by the filtered signal phase.

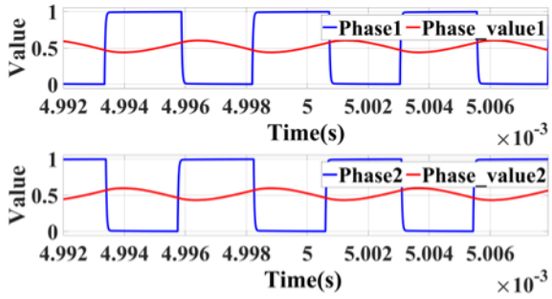

FIGURE 11. Pulse and filtered signals of the phase waveform

PHASE SHIFT

The simulated phase waveform of i_{m1} and i_{m2} are represented by phase1 and phase2 respectively. Both magnetizing currents are subject to Sallen-Key LPF process, which limits the magnetizing currents phase values to approximately 0.5 only. Figure 12 depicts the i_{m1} phase that accurately synchronizes with the i_{m2} phase. Thus, their magnitudes and phases are identical.

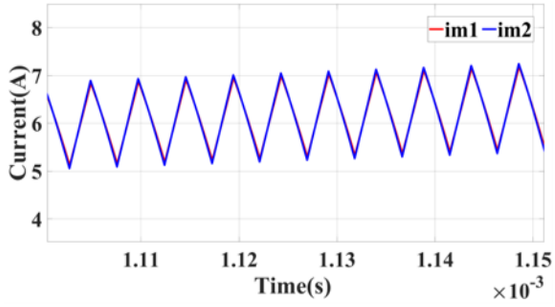

FIGURE 12. Synchronized i_{m1} and i_{m2}

The current switching time is fixed at 5 µs. It is the period gap between subsequent peaks of the triangular waveform. To reduce the ripples variation of output voltage, both currents require staggered tuning. Since the current is shifted for half-cycle period, the i_{m1} and i_{m2} phases are staggered apart by 180º. The phase shifted of i_{m1} and i_{m2} as illustrated in Figure 13 is obtained by utilizing the interleaved configuration in flyback circuit.

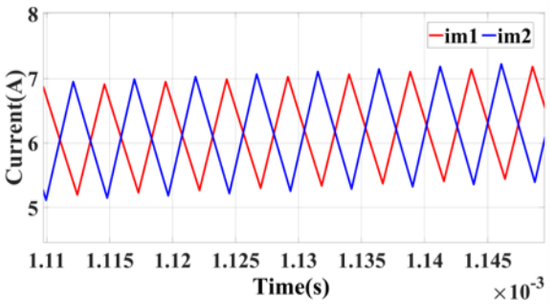

FIGURE 13. Phase shifted between i_{m1} and i_{m2}

HYSTERESIS CONTROL

The simulation results of hysteresis bands and i_{m1} are depicted in Figure 13. The i_{m1} shape is a sinusoidal waveform with constant ripple variation. It is sandwiched in between upper and lower hysteresis bands. Its minimum value is zero, while the maximum value is about 34 A. Based on the shape and peak-to-peak amplitude, it owns a rectified waveform property. Thus, the waveform of $i_{m1}$and i_{m2} are identical since their design procedure and parameters are the same.

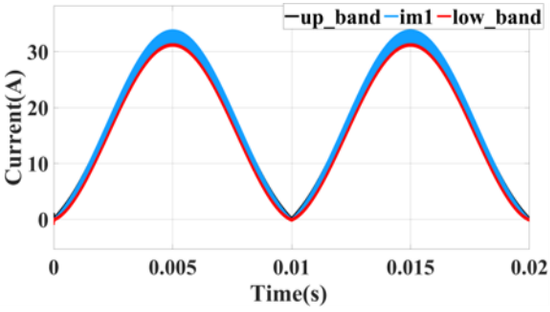

FIGURE 14. Magnetizing current is sandwiched in between two hysteresis bands

To investigate further about the ripple effect, the RHC waveform is zoomed in at 0.005s as shown in Figure 15. Obviously, both the upper and lower bands of the RHC demonstrate a ripple characteristic. With careful observation, the upper band ripple is 180º apart from the lower band ripple. On the other hand, HCC has not shown a ripple characteristic, but rather the straight upper and lower bands. This characteristic is depicted in Figure 15. Therefore, the magnetizing current switching frequency can be effectively controlled by the RHC since its rippled band is used for the trigger operation.

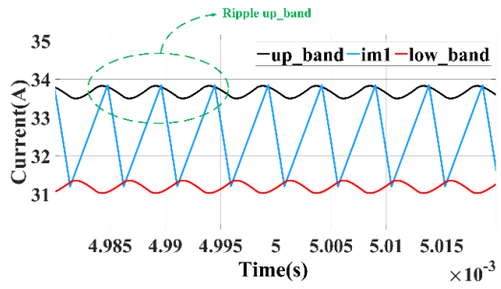

FIGURE 15. RHC using rippled bands

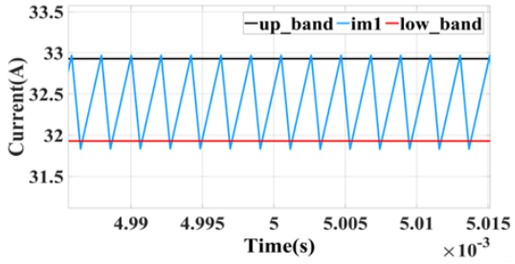

FIGURE 16. HCC using fixed bands

PRIMARY AND SECONDARY CURRENT

Due to the triggered frequency of the ripple hysteresis band is 200 kHz, hence the magnetizing current frequency is fixed at 200 kHz. Figure 16 simulates the primary current on the primary side of switching transformer in the flyback circuit. Whilst Figure 17 exhibits the behavior of secondary current of switching transformer. The interleaving phase is stable at both primary and secondary stages.

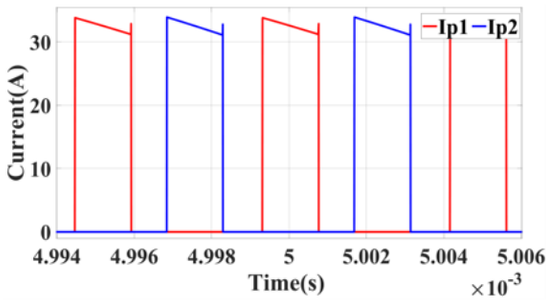

FIGURE 17. Primary current

Based on the simulation data, it has been decided that favourable operational outcomes can be carried out for the magnetizing current when it is triggered by the ripple hysteresis band. To enhance the circuit system and accurately compute its characteristics, it is imperative to establish the fixed frequency and phase of the magnetizing current using the ripple hysteresis band. In real-world hardware applications, precise parameters are indispensable

not only for comprehending the circuit's functionality but also for facilitating improvement initiatives.

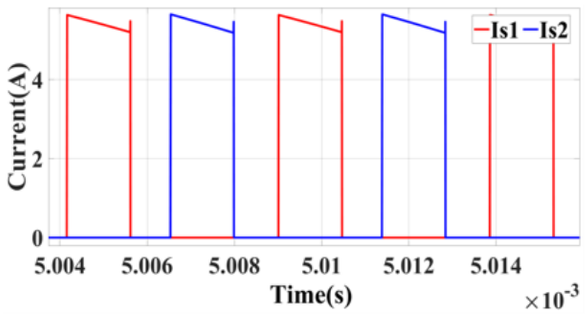

FIGURE 18. Secondary current

The waveform of the simulated AC output voltage for one cycle is depicted in Figure 18. It is a purely sinusoidal waveform. The AC output voltage of the flyback circuit under RHC has a peak value of 340 V, hence the RMS value is 240 V. The ripple effect is not significant throughout the AC voltage waveform since it only exists at each peak.

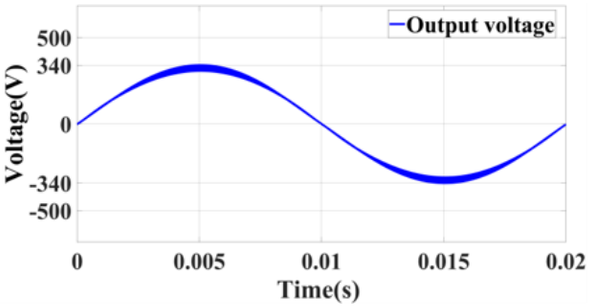

FIGURE 19. Sinusoidal AC output voltage

ANALYSIS AND DISCUSSION

This section analyzes and discusses the performance of the RHC and its counterpart via comparison. Based on Figs. 20 and 21, the i_m behaviour is analyzed. It was discovered that for the HCC case, when the i_m reaches zero-crossing point, it suddenly disoriented and jumps for a period of 0.3 ms, which leads to errors in phase and frequency. However, for the RHC case, the i_m in the ripple hysteresis band demonstrates a steady and smooth transition when it reaches the zero-crossing point. Therefore, the RHC has better performance in term of high switching frequency controllability as well as the i_m signal stability particularly at zero-crossing point.

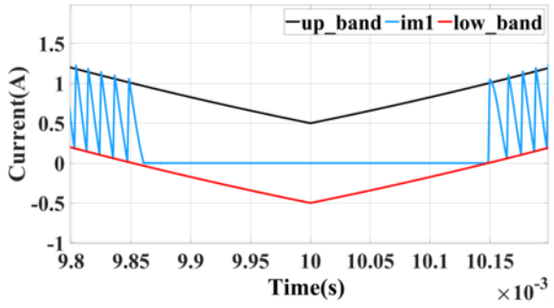

FIGURE 20. A sudden jump at zero-crossing for i_m signal

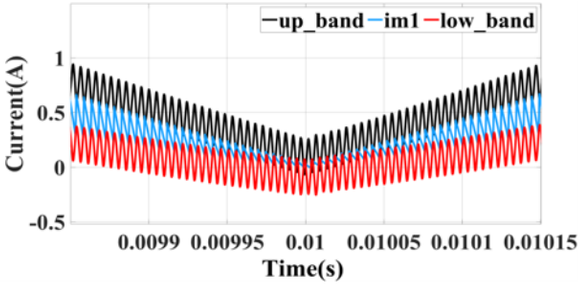

FIGURE 21. Smooth transition at zero-crossing for i_m signal

The AC output voltage waveforms under HCC and RHC are shown in Figs. 22 and 23, respectively. Both conventional and ripple hysteresis controls utilize a 200 kHz switching frequency, where the peak values from the same period are chosen for comparison. To confirm the performance of HCC, both the AC output voltage and magnetizing current are compared at the same time. Referring to a small portion of i_m in Figure 22, a bit tough to detect the simultaneous phase of i_m and V_{out}, due to the i_m peak ripple varies rapidly. Moreover, at zero-crossing line the V_{out} paused around 0.3 ms before entering the negative cycle.

The following equation is used to calculate the rate of voltage ripple amplitude variation at peak voltage.

$$r = \frac{RA}{V_m} \times 100\% \tag{16}$$

where r represents the rate of change of peak voltage, RA denotes the ripple amplitude of AC output voltage and V_m represents the amplitude of AC output voltage. Therefore, for HCC case, the measured RA is 47 V and the measured V_m is 348 V. Based on these measurements, the value of r is,

$$r = \frac{47}{348} \times 100\% = 13.5\%$$

Figure 22 compares the output voltage and current phase different values under RHC analytically. The RHC based AC output voltage ripple is smaller and consistent compared to the HCC. In addition, the phase angle of magnetizing current is fixed, also the phase staggering different value remained at 180º. The measured *RA* is 32 V, whereas the measured V_m is 340 V. Thus, the *r* can be estimated for RHC case,

$$r = \frac{32}{340} \times 100\% = 9.4\%$$

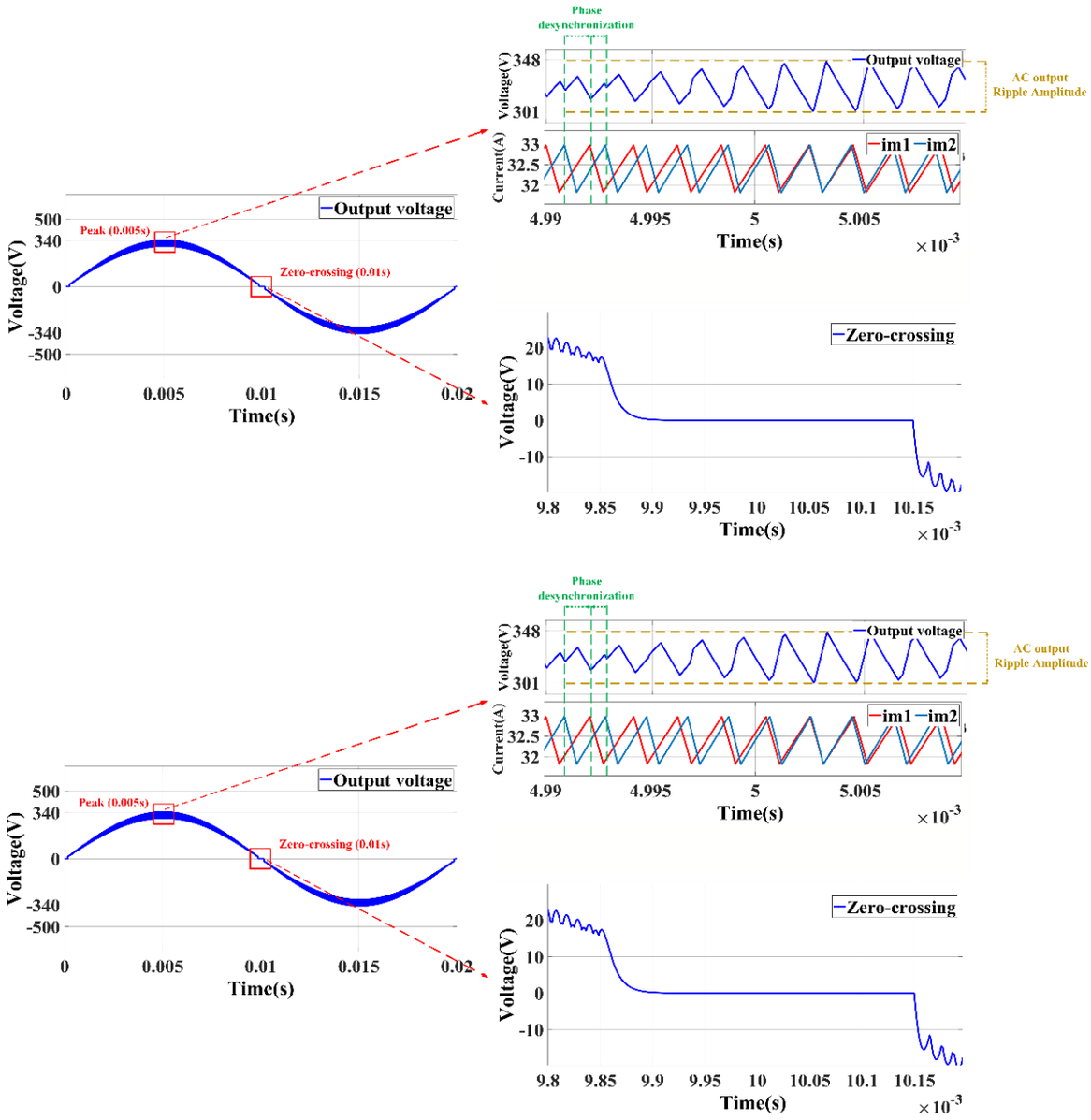

FIGURE 22. Output voltage and magnetizing current of HCC and their behaviour at zero-crossing and peak

The RHC yields a peak ripple change rate much less than the HCC. Meaning that the RHC has better ripple control than the conventional one. Moreover, the zero-crossing control of output voltage using the RHC is better compared to that of the HCC. For instance, at the moment the voltage crosses the zero crossing point, it immediately transfers from positive cycle to negative cycle. Thus, the voltage maintains consistent without any pause, simply a slight voltage drop of less than 2.0 V at exactly zero-crossing point.

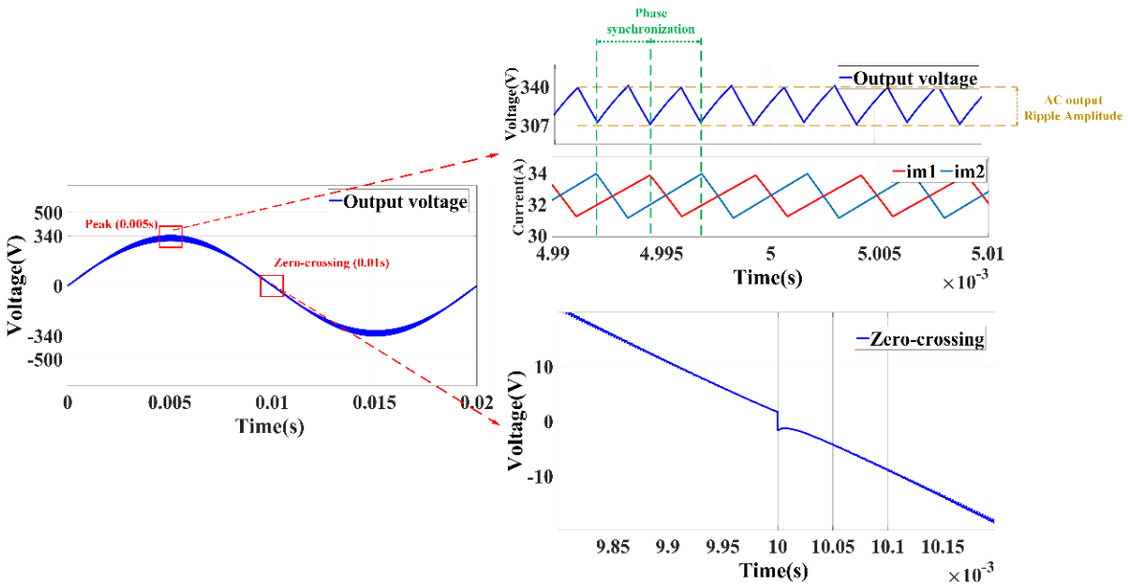

FIGURE 23. Output voltage and magnetizing current of RHC and their behaviour at zero-crossing and peak

In addition, Figure 24 illustrates the effect of asynchronous phase of two parallel secondary currents. The upper trace shows that the maximum amplitude of 5 A i_{s1} is repeatedly change phase, while its counterpart, the i_{s2} phase is periodically unchanged. It also shown that i_{s1} overlapped i_{s2} for several times. In other word, i_{s1} phase is faster than i_{s2} phase. The lower trace indicates the alternating capacitor current inconsistent truncated waveform with three levels magnitude. The amplitude in between the maximum peak and the minimum peak is 11.8 A. Initially, the truncated waveform is apparent, but after the fourth, its truncated waveform instantly disappear. This implies the asynchronous phase causing unstable control environment for the capacitor current.

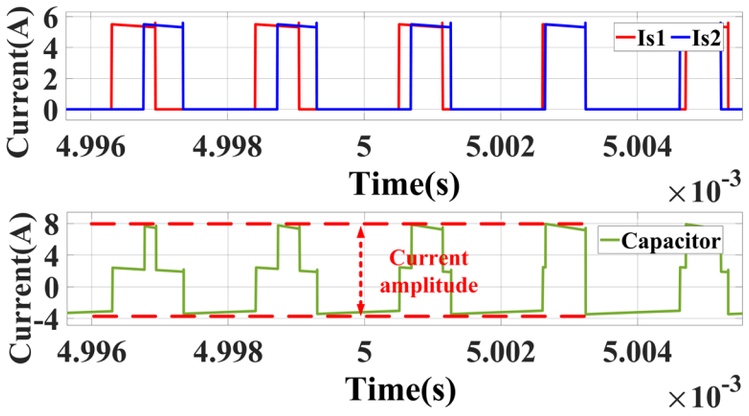

FIGURE 24. Effect of phase desynchronization on secondary and capacitor currents for HCC

The following Figure 25, on the other hand, illustrates the effect of RHC on the secondary currents (upper trace) and the capacitor current (lower trace) respectively. As a result of phase synchronization of secondary current in the parallel branch circuit. Clearly, both secondary currents i_{s1} and i_{s2} alternately keep changed their positions. They are complementing each others with constant maximum current value of 5 A. On the other hand, the capacitor current waveform is a consistent square wave. The amplitude difference of capacitor current is being reduced to 5.96 A, contrasted to the outcome of HCC in Figure 24.

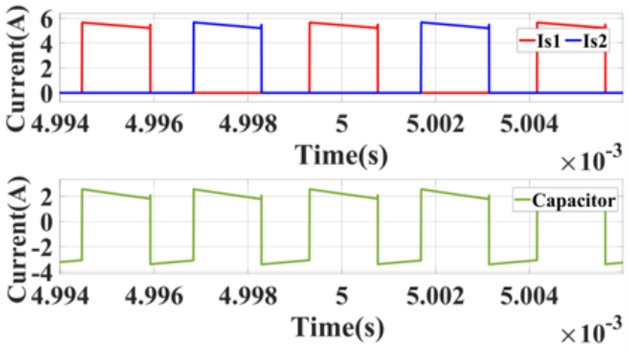

FIGURE 25. Effect of phase synchronization on secondary and capacitor currents for RHC

This explains the RHC causes the capacitor current and the secondary currents having a better control and stable operation without any overlap as compared to the HCC. Moreover, the substantial reduction in capacitor current amplitude signifies an enhanced effectiveness of RHC in managing current errors. Specifically, it demonstrates a remarkable 49.5% reduction in current error compared to the HCC. This outcome clarifies the superior performance of the RHC method, showcasing its capacity to significantly improve the precision and stability of current control within the main circuit.

Usually, the quality of inverter circuit output voltage is evaluated based on its harmonic distortion content. A common practice to measure harmonic distortion content is by utilizing a Total Harmonic Distortion (THD) term. Hence, the percentage of THD is summarized using the following expresssion,

$$THD = \frac{\sqrt{V_{n\neq1}^2}}{V_1} \tag{17}$$

where V_n is the RMS value of nth harmonic voltage, V_1 is the RMS value of the harmonic voltage fundamental component while n is the number of harmonic order.

The THD spectrum of output voltage for the respective HCC and RHC are depicted in Figure 26. In this analysis, the maximum frequency is limited to 3000 Hz or 60th

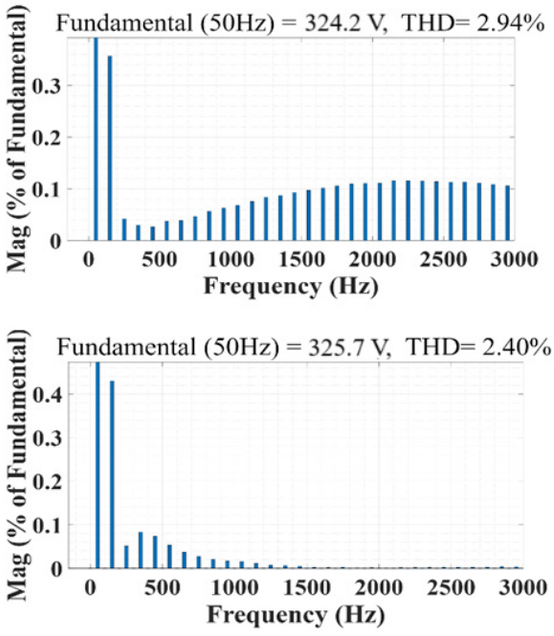

FIGURE 26. Voltage THD spectrum for HCC (upper) and RHC (lower)

harmonic order, where the fundamental frequency is 50 Hz. The upper bar graph in Figure 26 shows the THD spectrum of the output voltage under the influence of HCC. In this case, the calculated output voltage THD is 2.94%. Usually, the highest magnitude after the fundamental is the third harmonic, which its magnitude reaches almost 0.36%, whereas the rest tends to raise gradually with increasing frequency.

On the other hand, the lower bar graph which pertinent to the RHC, indicates the measured output voltage THD is only 2.4%. The THD difference between RHC and HCC is 0.54%. Its third harmonic magnitude is the highest after the fundamental, close to 0.44%. Nevertheless, the subsequent harmonic orders magnitude are declining with increasing frequency until they totally disappearad at 1500 Hz onwards. Therefore, by comparison the THD of the RHC is lowered by 18.4% than the HCC. These findings highlights the efficient performance of RHC in term of voltage harmonic control and the output voltage quality, which obviously superior than the HCC.

Table 3 presents a comparative analysis of simulated outcomes between the HCC and the RHC. This comparison aims to provide a summary achievements for RHC, particularly emphasizing its superior performance over HCC in flyback inverter. The table includes several key parameters to quantitatively and qualitatively indicate the effective performance of RHC in relation to the HCC approach.

TABLE 3. Performance comparison between HCC and RHC

Parameters	HCC	RHC	RHC reduction percentage (%)
Voltage peak (V)	348 V	340 V	2.3
Peak voltage ripple change percentage (%)	13.5%	9.4%	41
Phase shift (°)	varied	180° (fixed)	100
Switching frequency (kHz)	varied	200 kHz (fixed)	100
THD (%)	2.94%	2.4%	18.4
Capacitor current amplitude (A)	11.8 A	5.96 A	49.5

CONCLUSION

This paper introduced a new flyback inverter circuit-based ripple hysteresis controller, presenting both the conceptual framework and simulation results. In general, the proposed RHC has better performances over the HCC while maintaining the qualities of simplicity and rapid response. It enables the hysteresis controller to successfully handle the frequency and phase of the magnetizing current signal, the issues that other hysteresis controllers have so far failed to accomplish. Moreover, the output voltage ripple amplitude is significantly reduced. This indirectly verifies the accuracy of the calculations and narrows the impact of unwanted errors introduced by the estimated data, both of which have a positive effect on the circuit's performance.

The proposed RHC leverages the hysteresis band as a trigger condition for current control. Notably, it achieves positive control over both the frequency and phase of current, while preserving the simplicity inherent from traditional hysteresis controllers. By direct comparison under identical conditions, the simulation results indicate that the RHC outperforms its traditional counterpart in several ways. It demonstrates enhanced effectiveness in controlling the amplitude of current ripple and accurately determining zero-crossing points. This not only results in reduced current errors but also furnished precise system parameters. The findings highlight the potential of RHC as a robust, alternative and efficient switching scheme, offering improved control capabilities for many power converter circuit applications.

Nevertheless, the RHC exhibits certain limitations that require further attention and resolution. One notable issue for improvement is the distortion observed in the output voltage and current under the RHC, particularly at low frequency. Abnormal fluctuations are also noted at zero-crossing and peak current, indicating a need for further exploration. Additionally, the introduction of new components to filter the control phase creates a time delay error. This complexity necessitates the analytical adjustment of multiple system parameters in both

simulations and real experiments. To address this, requires simplified system parameters while upholding optimal control performance. Besides, to validate further, a flyback inverter circuit utilizing RHC scheme will be developed and its actual performance will be tested via laboratory experiment.

In conclusion, the RHC introduced a novel solution concept for addressing switching frequency problems within hysteresis control approach. Even though it represents a promising advancement, it still has sizeable space for research and development works. Overall, the proposed RHC proves a significant positive impact for the flyback inverter circuit's switching scheme as well as promising a great opportunity for more in-depth and useful applications in the future.

ACKNOWLEDGEMENT

The authors acknowledge the Ministry of Higher Education Malaysia (MOHE) by funding this research through fundamental research grant scheme, FRGS/1/2018/TK04/UKM/03/4, as well as the UKM for providing the financial support under GP-K010180 grant scheme.

DECLARATION OF COMPETING INTEREST

None.

REFERENCES

Bhattacharya, A., Paul, A.R. & Chatterjee, K. 2023. A coupled inductor based ćuk microinverter for single phase grid connected PV applications. *IEEE Transactions on Industry Applications* 59(1): 981–993.

Chen, M., Zheng, R., Fu, Y., Qi, J., Han, F., Jiang, F. & Yao, W. 2021. An analog control strategy with multiplier-less power calculation circuit for flyback microinverter. *IEEE Transactions on Power Electronics* 36(8): 8617–8621.

Can, E. 2019. The load performance of multi-level alternating voltage provided by upgrade effect. *Jurnal Kejuruteraan* 31(2): 249–259.

Dong, Z., Song, Z., Wang, W. & Liu, C. 2023. Improved zero-sequence current hysteresis control-based space vector modulation for open-end winding PMSM drives with common DC bus. *IEEE Transactions on Industrial Electronics* 70(10): 10755–10760.

Feng, Y. & Li, Y. 2021. System identification of micro piezoelectric actuators via rate-dependent Prandtl-Ishlinskii Hysteresis Model based on a modified PSO algorithm. *IEEE Transactions on Nanotechnology* 20: 205–214.

Ghani, Z.A., Rosli, S.S. & Othman, H. 2022. Modeling and implementation of photovoltaic modules for a DC-DC boost converter. *Jurnal Kejuruteraan* 5(2): 225–231.

Kapat, S. 2017. Parameter-insensitive mixed-signal hysteresis-band current control for point-of-load converters with fixed frequency and robust stability. *IEEE Transactions on Power Electronics* 32(7): 5760–5770.

Komurcugil, H., Bayhan, S. & Abu-Rub, H. 2017. Variable- and fixed-switching-frequency-based HCC methods for grid-connected VSI with active damping and zero steady-state error. *IEEE Transactions on Industrial Electronics* 64(9): 7009–7018.

Lee, S.-H., Cha, W.-J., Kwon, J.-M. & Kwon, B.-H. 2016. Control strategy of flyback microinverter with hybrid mode for PV AC modules. *IEEE Transactions on Industrial Electronics* 63(2): 995–1002.

Li, X., Liu, Y. & Zhang, H. 2023. Hybrid-modulation hysteresis scheme based decoupled power control of grid-connected inverter. *IEEE Journal of Emerging and Selected Topics in Power Electronics* 11(1): 276–287.

Liang, H.W.R., Yang, Y., He, L., Qu, J., Lee, C.K. & Hui, S.Y.R. 2023. A multi-hysteresis control for minimizing battery charging time within industrial JEITA guidelines. *IEEE Transactions on Industrial Electronics* 70(8): 8416–8425.

Matharani, K. & Jariwala, H., 2024. Design of fuzzy logic based adaptive active power controller to enhance power sharing among DGs in an autonomous microgrid. *Jurnal Kejuruteraan* 36(1) 2024: 273-285

Ma, Y., Zhang, G. & Tong, M.S. 2020. A wide input range subsampling phase detector in subsampling phase locked loop. *2020 IEEE International Conference on Computational Electromagnetics (ICCEM).*

Peter, J., KP, M.S., R, L. & Ramchand, R. 2020. Online boundary computation using sampled voltage reference for bus clamping PWM-based hysteresis-controlled VSI-fed IM drive. *IEEE Transactions on Power Electronics* 35(4): 3939–3950.

Repecho, V., Biel, D., Olm, J.M. & Colet, E.F. 2017. Switching frequency regulation in sliding mode control by a hysteresis band controller. *IEEE Transactions on Power Electronics* 32(2): 1557–1569.

Rovere, L., Formentini, A., Calzo, G.L., Zanchetta, P. & Cox, T. 2019. Zero-sequence voltage elimination for dual-fed common DC-link open-end winding PMSM high-speed starter-generator—Part II: Deadtime

hysteresis control of zero-sequence current. *IEEE Transactions on Industry Applications* 55(6): 7813–7821.

Sibanyoni, M. & Daniel Chowdhury, S.P. 2017. Synchronization strategy for single phase inverters for feeding renewable energy in South African National Grid. *2017 52nd International Universities Power Engineering Conference (UPEC)*.

Shi, H., Zhang, Z., Han, J. & Li, J. 2023. Dynamic performance improvement of wound rotor synchronous starter/generator system based on PWM rectifier. *IEEE Transactions on Transportation Electrification* 9(3): 4639–4649.

Wang, Y., Ruan, X., Leng, Y. & Li, Y. 2019. Hysteresis current control for multilevel converter in parallel-form switch-linear hybrid envelope tracking power supply. *IEEE Transactions on Power Electronics* 34(2): 1950–1959.

Wang, Z., Yan, Y., Yang, J., Li, S. & Li, Q. 2019. Robust voltage regulation of a DC–AC inverter with load variations via a HDOBC approach. *IEEE Transactions on Circuits and Systems II: Express Briefs* 66(7): 1172–1176.

Wang, K.-J., Sun, H.-C. & Cui, Q.-C. 2020. The fractional sallen-key filter described by local fractional derivative. *IEEE Access* 8: 166377–166383.

Yan, Y., Wang, T., Wang, Y., Zhu, M., Tang, H. & Qian, Q. 2023. Adaptive dead-time and partial-ZVS regulation for GaN-based active clamp flyback converter with predictive hysteresis current mode control. *IEEE Transactions on Power Electronics* 38(9): 10782–10797.

Yusof, Y. & Rahim, N.A. 2011. Functional simulation model for single phase Pulse Width Modulation-Voltage Source Inverter (PWM-VSI) using switching function concept. *Jurnal Kejuruteraan* 23: 49-56.

Yusof, Y. & Rahim, N.A. 2011. Comparative study between SPWM and THIPWM control techniques for PWM-VSI using mathematical modeling and simulation. *Jurnal Kejuruteraan* 23: 17-26.

Zainuri, M. A. M, Azari, E.A., Ibrahim, A.A., Yusof, Y. & Radzi, M.A.M. 2019. Analysis of adaptive perturb and observe-fuzzy logic control maximum power point tracking for photovoltaic boost DC-DC converter. *International Journal of Advanced Trends in Computer Science and Engineering* 8(1.6 Special Issue): 201–210, 31.

Zhang, Z., Zhang, J., Shao, S. & Zhang, J. 2019. A High-efficiency single-phase t-type BCM microinverter. *IEEE Transactions on Power Electronics* 34(1): 984–995.

Za'im, R., Jamaludin, J. & Rahim, N.A. 2019. Photovoltaic flyback microinverter with tertiary winding current sensing. *IEEE Transactions on Power Electronics* 34(8): 7588–7602.

Za'im, R., Jamaludin, J., Yusof, Y. & Rahim, N.A. 2022. High step-up flyback with low-overshoot voltage stress on secondary GaN rectifier. *Energies* 15(14): 5092.